

Factor XII and kininogen asymmetric assembly with gC1qR/C1QBP/P32 is governed by allostery

Bubacarr G Kaira^{1†}, Alexandre Slater^{2†}, Keith R McCrae³, Ingrid Dreveny¹, Sumya Ummay⁴,
Nicola J Mutch⁴, Mark Searle², & Jonas Emsley^{1*}

† BGK & AS contributed equally to this work and are co-first authors

* JE & MS are co-last/corresponding authors

School of Pharmacy, Centre for Biomolecular Sciences, University Park, University of Nottingham, Nottingham NG7 2RD, UK

School of Chemistry, Centre for Biomolecular Sciences, University Park, University of Nottingham, Nottingham NG7 2RD, UK

Departments of Hematology and Oncology and Cellular and Molecular Medicine, Cleveland Clinic, USA.

Aberdeen Cardiovascular & Diabetes Centre, School of Medicine, Medical Sciences & Nutrition, Institute of Medical Sciences, University of Aberdeen, Aberdeen, AB25 2ZD.

Corresponding authors: jonas.emsley@nottingham.ac.uk, mark.searle@nottingham.ac.uk

Abstract word count: 250

Text word count: 3933

Number of figures 7

tables: 2

Number of references: 50

Running title: FXII-gC1qR complex structure

Scientific category: Thrombosis and Haemostasis

Abbreviations: Plasma kallikrein (PK), High molecular weight kininogen (HK), Factor XII (FXII), Factor XI (FXI), Factor IX (FIX), complement C1q binding protein (gC1qR), Protein Data Bank (PDB).

Abstract

The contact system is composed of Factor XII (FXII), prekallikrein (PK) and co-factor kininogen (HK). The globular C1q receptor (gC1qR) has been shown to interact with FXII and HK. We reveal the FXII fibronectin type II domain (FnII) binds gC1qR in a Zn²⁺ dependent fashion and determined the complex crystal structure. FXIIFnII binds the gC1qR trimer in an asymmetric fashion with residues Arg36 and Arg65 forming contacts with two distinct negatively charged pockets. gC1qR residues Asp185 and His187 coordinate a Zn²⁺ adjacent to the FXII binding site and a comparison with the ligand free gC1qR crystal structure reveals the anionic G1-loop becomes ordered upon FXIIFnII binding. Additional conformational changes in the region of the Zn²⁺ binding site reveal an allosteric basis for Zn²⁺ modulation of FXII binding. Mutagenesis coupled with SPR demonstrate the gC1qR Zn²⁺ site contributes to FXII binding and plasma based assays reveal gC1qR stimulates coagulation in a FXII-dependent manner. Analysis of the binding of HK domain 5 (HKD5) to gC1qR shows only one high affinity binding site per trimer. Mutagenesis studies identify a critical G3-loop located at the center of the gC1qR trimer suggesting steric occlusion as the mechanism for HKD5 asymmetric binding. Gel filtration experiments reveal that gC1qR clusters FXII and HK into a higher order 500kDa ternary complex. These results support the conclusion that extracellular gC1qR can act as a chaperone to cluster contact factors which may be a prelude for initiating the cascades which drive bradykinin generation and the intrinsic pathway of coagulation.

KEY POINTS

Crystal structure of the Factor XII fibronectin type II domain in complex with gC1qR reveals an asymmetric interaction and bound Zn²⁺ ions

gC1qR clusters Factor XII and kininogen into higher order ternary complexes

KEY WORDS

Plasma kallikrein, Factor XII, Globular complement C1q receptor, Kininogen

Introduction

The contact activation system lies at the crossroads of plasma coagulation and innate immunity and consists of proteases factor XII (FXII), prekallikrein (PK) and co-factor high molecular weight kininogen (HK)¹⁻³. Binding of contact factors to the cell surface has been shown to be mediated by the complement C1q receptor (gC1qR also known as C1QBP, HABP1, P32) and the urokinase receptor (uPAR)⁴⁻⁷. gC1qR is a multi-compartmental and multi-functional protein essential for mitochondrial function⁸, but is also present at the surface of stimulated cells⁹⁻¹¹. gC1qR has no plasma membrane anchor but forms interactions with other cell surface proteins and receptors (cytokeratin-1, β_1 -integrin, DC-specific ICAM-3-grabbing nonintegrin receptor, fibrinogen)^{4,12-15}. The gC1qR crystal structure is a doughnut shaped symmetrical trimer with both a highly acidic ligand binding surface and a cell binding face¹⁶. gC1qR has been characterized as binding a diverse array of structurally distinct ligands^{7,9,15,17,18} and has been proposed to function as a chaperone directing the assembly of multiprotein complexes¹⁹.

The domain structures of FXII, HK and gC1qR are shown in Figure 1a. Crystal structures have been determined for the FXII protease domain²⁰⁻²² and the fibronectin type I (FnI) and epidermal growth factor-like domains (EGF)²³. As the N-terminal FXIIFnII domain is central to understanding processes of FXII conformational regulation²⁴ we determined the crystal structure in complex with gC1qR. This revealed an asymmetric FXII binding mode and a novel Zn²⁺ binding site in the gC1qR structure.

Experimental Procedures

Protein Expression and Purification

The human gC1qR (residues 74-282 with Leu74 substituted to Met74) *E.coli* expression vector was a gift from Dr Adrian R. Krainer, Cold Spring Harbor Laboratory, USA. Expression and purification of gC1qR was performed as described¹⁶. gC1qR variants were generated by site-directed mutagenesis using the Agilent technologies QuikChange kit. HKD5 was expressed in *E.coli* using the pET28a vector and D5-1, D5-2, HK 401-438 were expressed as GST fusion proteins using the pGEX 4T-1 vector (Supplemental Figure 1). Untagged FXIIFnII domain (residues 1-71) was cloned into vector

pMT-PURO for expression in the insect cell based DES system (Invitrogen) using previously described protocols²². FXIIFnII was initially purified from media using a Capto-S column (GE healthcare) equilibrated with 0.05 M MES pH 6.0 and a gradient of 0-1.0 M NaCl was used for elution. Subsequently, this was applied to a HiTrap Ni²⁺ column (GE Healthcare) and eluted using an imidazole gradient concentration of 0-1.0 M and a final purification step of gel filtration with a HiLoad SuperdexTM 75 16/60 column (GE healthcare) in 0.05 M Tris-HCl pH 8.0 and 0.1 M NaCl (Supplemental Methods).

Crystallization, data collection and structure determination

FXIIFnII was mixed with gC1qR and 50 μ M ZnCl₂ and the complex was isolated using a SuperdexTM increase 200 10/300 column equilibrated with 0.02 M HEPES pH 7.4, 0.14 M NaCl (Figure 1c). FXIIFnII-gC1qR complex fractions were collected and concentrated to 5.3 mg/ml. Crystals were obtained in 0.1 M NaCacodylate pH 5.5, 0.1 M CaAc₂, 12% (w/v) PEG 8000 at 10 °C. A dataset for a single FXIIFnII-gC1qR complex crystal was collected and processed using the CCP4 suite and the structure determined by molecular replacement with Phaser²⁵ and the gC1qR structure (PDB:1P32) as a template. Model building (COOT) and refinement (REFMAC)²⁶ provided a final refined model containing the gC1qR trimer, FXIIFnII and three Zn²⁺ (Table 1).

Surface Plasmon Resonance (SPR)

Plasma purified FXII was purchased from Enzyme Research Laboratories and immobilised onto a CM5 chip using an amine coupling kit (GE healthcare) and experiments were performed on a Biacore® 3000 instrument. The running buffer was 0.02 M HEPES pH 7.4, 0.14 M NaCl and 50 μ M ZnCl₂ and the chip surface was regenerated with 1M NaCl, 0.02 M EDTA. To assess any non-specific binding, the analyte (gC1qR) was also injected over an empty flow cell. Binding curves were analysed on the basis of the SPR response units recorded at equilibrium for each analyte protein concentration and a Hill plot was generated using Prism 6 (GraphPad Software Inc.).

Isothermal Titration Calorimetry (ITC)

A MicroCal VP ITC system (Malvern) was used for all ITC experiments performed at 25°C. The ITC cell contained 1.4 mL of *wt*-gC1qR or gC1qR variant whilst 300 µL of D5 ligand was loaded into the syringe. The reference power was set at 5 µcal/sec, and the syringe stirring speed was set at 300 rpm. An initial pre-equilibration step of 1 hour was followed by 30 x 10 µL injections. Ligand dilution effects were tested by running a ligand to buffer control using the same titration parameters. The ligand to buffer control was subtracted from the experimental data, and any anomalous titration points were removed. Curves for D5-2 and HK 493-516 were fit to a one binding site model, whereas curves for D5 and D5-1 were fit to a three site sequential binding model (Table 2).

Plasma based coagulation assays

Blood was drawn from healthy volunteers into vacuettes (Greiner Bio-One Ltd) containing 3.2 % sodium citrate. To isolate platelet poor plasma, tubes were spun at 1860 x *g* for 30 min at 4°C. Pooled normal plasma (PNP) was derived from at least 20 donors, aliquoted and stored at -70°C. Ethical approval was obtained from the University of Aberdeen College Ethics Review Board. The activated Partial Thromboplastin Time (aPTT) assay was performed in a STart 4 coagulometer (Diagnostica Stago). PNP ± gC1qR (50-200 µg/ml) was incubated with PTT Automate reagent (Stago UK, Theale, England) and Zn²⁺ (50 µM) at 37°C for 180 s. Clotting was initiated by addition of CaCl₂ (0.0083 M). Thrombin generation was measured in Calibrated Automated Thrombinoscope. PNP, FXII or Factor XI (FXI) deficient plasma (Hypen Biomed, France) ± gC1qR (50-200 µg/ml) and Zn²⁺ (50 µM) were added to thrombin calibrator and MP reagent (Stago UK, Theale, England) in Greiner 96-well plates. The plate was incubated for 10 min followed by addition of FluCa solution, as per manufacturer guidelines. Thrombinoscope software package (Synapse Bv, Maastricht, Netherlands) was used to quantify real-time thrombin activity.

Data sharing statement

The FXIIFnII-gC1qR complex crystal structure has been deposited in the PDB (www.rcsb.org) with accession code 6SZW.

Results

Structure of the FXIIFnII-gC1qR complex

Recombinant FXIIFnII domain (residues 1 to 71) was produced in insect cells and was shown using gel filtration to bind gC1qR in the presence of 50 μ M ZnCl₂ (Figure 1b,c). Complex formation was not observed at lower ZnCl₂ concentrations, consistent with the previous report by Joseph *et al.* on the Zn²⁺ dependency of FXII binding to gC1qR⁷. The FXIIFnII-gC1qR structure was determined to 3 \AA resolution (Table 1, Figure 1d). Figure 1e shows FXIIFnII has an asymmetric binding mode and unexpected stoichiometry of one FXIIFnII bound to the gC1qR trimer. The asymmetry of binding is achieved in part by the Arg36 and Arg65 side chains of FXII reaching out via the guanidinium groups to form contacts with distinct gC1qR negatively charged pockets termed G1 and G2 (Video 1,2). gC1qR pocket G1 consists of anionic residues 190-202 (termed the G1-loop) together with residues Tyr236 from the α B helix and Trp233, Asp229 from the α B- β 7 loop burying a surface area of 489 \AA^2 . The FXIIFnII β 2 strand forms main chain to main chain interactions resulting in an anti-parallel β -sheet contact with gC1qR residues Glu198-Ser201 (Figure 2a,b). Electrostatic complementarity occurs via negatively charged side chains from gC1qR (Asp197, Asp229) forming salt bridge interactions with FXII side chains Lys45 and Arg36, respectively. At the tip of the FXIIFnII β 1- β 2 hairpin the Arg36 side chain forms further hydrogen bonds to the main chain carbonyl of Thr228 and a cation- π interaction with the side chain of Tyr236. Central hydrophobic contacts are made by the side chain of FXII Tyr39 with gC1qR Ala199 and flanking this FXII Gln37 hydrogen bonds to the side chain of gC1qR Ser201 (Figure 2b).

The FXII Arg65 side chain utilizes the guanidinium group to form interactions with three gC1qR residues; a salt bridge to Asp249, a hydrogen bond to the Gly247 main chain carbonyl, and hydrogen bonds to the Ser106 main and side chain (labeled G2 pocket in Figure 2c). Additional gC1qR G2 pocket interactions occur with FXII residues Asp63, Gln64 forming a salt bridge and hydrogen bond to the gC1qR Arg122 side chain and Ser106 main chain nitrogen, respectively burying

a total surface area of 238Å². In between the G1 and G2 pockets a hydrophobic contact is formed between the FXIIFnII Gln62 and the gC1qR Trp233 side chain (Figure 2d).

Quantitation of FXII-gC1qR ligand binding

The FXIIFnII-gC1qR structure is consistent with previous ELISA data from Gebrehiwet *et al.* showing the single point mutation of gC1qR Trp233Gly and G1-loop deletion variants disrupted FXII binding²⁷. The involvement of the gC1qR G2 pocket residues in the interaction with FXII is novel and we developed an SPR assay to quantitate the gC1qR-FXII interaction with a series of gC1qR variants. Plasma purified full-length FXII was amine-coupled to a CM5 sensor chip (GE Healthcare) and a reference cell was prepared by blank amine-coupling. A recombinant gC1qR wild-type (*wt*-gC1qR) dilution series was conducted and analysis of sensorgrams resulted in a K_D of 120±12 nM in the presence of 50 µM ZnCl₂ (Figure 3a). Consistent with the gel filtration data, no complex was observed in the absence of Zn²⁺ or with EDTA in excess (5 mM). To test the contribution of the gC1qR G1 and G2 pockets to binding FXII we prepared two gC1qR variants replacing key residues with alanine; T228A, D229A, W233A, Y236A (variant gC1qR-G1-4Ala) and S106A, D249A (gC1qR-G2-2Ala). The structural integrity of the recombinant gC1qR variants was confirmed by gel filtration revealing native-like characteristics of the trimer. Both the gC1qR G1 and G2 pocket variants failed to elicit a significant signal response or a clear association binding curve under the same conditions of the SPR binding assay to FXII illustrating the contribution of residues from the G1 and G2 pocket to FXII binding (Figure 3b,c).

Zn²⁺ binding to the gC1qR receptor induces a conformational change

Kumar *et al.* showed gC1qR displays specific binding to Zn²⁺ ions²⁸ and divalent cations such as Ca²⁺ and Mg²⁺ do not bind or support formation of the complex with FXII. Utilizing the structure factors collected for the FXIIFnII-gC1qR complex we observed the three highest peaks in an anomalous difference Fourier map were consistent with a Zn²⁺ coordinated by residues Asp185 and His187. The measured bond lengths are consistent with Zn²⁺ tetrahedral coordination geometry with two water molecules also bound. To test the contribution of the gC1qR Zn²⁺ binding site to FXII

binding we prepared a gC1qR H187A variant. SPR experiments were used to assess binding to immobilized full-length FXII and revealed attenuated binding of gC1qR H187A compared to *wt*-gC1qR which could not be fitted to derive a K_D (Figure 3d). The Zn^{2+} is located close to the base of the acidic G1-loop adjacent to the FXIIFnII binding site (Figure 3e). In the previously published gC1qR crystal structure (PDB:1P32¹⁶) no metal ion is observed bound at the Asp185-His187 site. We also determined a 1.7 Å resolution gC1qR structure in the presence of Ca^{2+} ions and as expected no metal ion was bound between residues His187 and Asp185 (unpublished results).

A comparison of the ligand free gC1qR structures with the FXII-gC1qR complex reveals that the Zn^{2+} is replaced by the Arg207 side chain which forms a salt bridge with Asp185 (Figure 3f). Arg207 does not directly contact FXII but in the FXII-gC1qR complex it forms a salt bridge to Glu190 which could indirectly influence FXII binding via the G1-loop. The Trp233 side chain is observed to have multiple conformations in the unbound crystal structures and resembles a flexible tip of the thumb-like helix αB which can open and close to allow ligand access to the G1-pocket (Video 3). The other major difference is that the anionic G1-loop becomes ordered upon FXIIFnII binding and this loop is not resolved in the unbound gC1qR crystal structures and is assumed to be flexible. These two sets of conformational changes in the region of the G1-pocket suggest an indirect/allosteric basis for the Zn^{2+} modulation of FXII binding.

HKD5 binding to gC1qR

HK binding to gC1qR has been quantified by a number of different techniques^{7,29-32} and SPR data in the study published by Pixley *et al.* revealed that binding to full-length HK was in the range 0.7–0.8 nM which could be abolished in the presence of chelating agent EDTA³³. The HKD5 domain and constituent peptides have been characterized as the key cell and Zn^{2+} binding³⁴⁻³⁶ sites of HK. To build on this previous data and conduct fine mapping of HKD5 binding regions and determine the stoichiometry of the interaction with the gC1qR trimer we expressed a series of HKD5 constructs (Figure 4a). Using gel filtration we were able to detect the co-elution of the HKD5-gC1qR complex when applied mixed in a 2:1 ratio whereas a 3:1 ratio revealed excess unbound HKD5 eluting separately (Figure 4b). To explore this further we utilized ITC with gC1qR in the sample cell titrated

with HKD5. These data confirmed that HKD5 binds to gC1qR in the absence of Zn^{2+} , and binding was unaffected by an excess of EDTA in the ligand buffer (Figure 4c). Examination of the binding isotherm revealed a multi-step binding curve which could be modeled as three sequential binding steps with very different affinities (K_{DS} of ~ 1.9 nM, ~ 64.9 nM and ~ 1.01 μ M). The symmetrical gC1qR trimer is therefore unable to accommodate HKD5 at the three equivalent sites, demonstrating allosteric effects between sites resulting in asymmetric binding. The first event is of high affinity (K_D of ~ 1.9 nM), and is associated with a strongly exothermic interaction and a compensating negative entropy change, typical of the binding and immobilization of a flexible ligand (Table 2). The second and third binding events are 35-fold and 500-fold weaker with much diminished enthalpy and entropy changes, consistent with partial steric occlusion at these two sites once the first high affinity site is occupied.

HKD5 Zn^{2+} dependent component to gC1qR binding

To determine the origin of the allosteric component of the interaction, we expressed recombinant N and C-terminal fragments of HKD5 in which D5-1 (residues 401-473) contains the His-Gly rich region and D5-2 (residues 474-531) is His-Gly-Lys-rich (Figure 4a). HKD5 has a His-rich nature (21% of the HKD5 sequence) and has previously been shown to bind Zn^{2+} ions^{34,35}. Using electrospray ionization mass spectrometry (ESI-MS) with the whole HKD5 we detected polypeptide species with 1, 2 and 3 bound Zn^{2+} ions and two Zn^{2+} bound in each case to D5-1 and D5-2 constructs respectively (Supplemental Figure 3-5).

We examined the binding of the D5-1 and D5-2 fragments to gC1qR by gel filtration and showed that both components could bind independently. The co-elution of the N-terminal D5-1 with gC1qR had a Zn^{2+} ion-dependency, whereas D5-2 did not. Co-elution of D5-1 with gC1qR could be eliminated in the presence of EDTA, but D5-2 was unaffected by EDTA (Figure 4d). This was confirmed by ITC measurements, in which titrations in buffer containing EDTA, eliminated the interaction with D5-1 but had no effect on D5-2 (Figure 4e,f).

The binding isotherms of the two fragments also showed highly distinct ITC profiles with HKD5-1 retaining the complex 3-phase binding curve observed for full-length HKD5, whereas the C-

terminal D5-2 fragment could be modeled as a single phase binding event, with an estimated stoichiometry of between 2 and 3 (N-value of 2.3) gC1qR sites each with a K_d of ~763.4 nM. The three-phase interaction of D5-1 with gC1qR showed a >40-fold reduction in affinity for the first high-affinity step compared with full-length HKD5, but only a 25 to 3-fold reduction for the lower affinity steps 2 and 3. These data show that the allosteric effects are largely associated with the His-Gly-rich D5-1 motif and occur in a Zn^{2+} -dependent manner (Table 2). The observation that the D5-2 fragment binds in a Zn^{2+} -independent fashion suggests that this basic His-Gly-Lys-rich D5-2 motif may be interacting at a different location on the gC1qR structure to D5-1. In the presence of Zn^{2+} we were able to detect a tri-complex between gC1qR, D5-1 and D5-2 by gel filtration with all components co-migrating in the same fractions (Figure 4d).

To further delineate the site of interaction on D5 we considered still shorter peptide motifs derived from D5-1 (HK residues 401-438, HK 439-455, HK 457-475) and D5-2 (HK 493-516) and studied the interaction by ITC. None of the peptides derived from D5-1 revealed any binding in the presence or absence of Zn^{2+} ions to gC1qR, suggesting that the binding site covers a much larger proportion of the D5-1 fragment (Figure 4g). However, the His-Gly-Lys-rich peptide HK 493-516 derived from D5-2 produced a Zn^{2+} independent single site binding isotherm comparable to that for D5-2, differing by only 2-fold in binding affinity, which similarly indicated ~3 equivalent sites on the gC1qR trimer. The HK 493-516 sequence resembles other peptides rich in Gly-Lys which have been characterized as binding to gC1qR^{37,38} without Zn^{2+} and an alignment of these sequences is shown in Supplemental Figure 7c.

A central gC1qR loop is utilized for HKD5 binding

Ghebrehiwet *et al.* utilized deletion mutants to identify gC1qR residues 144-148 and 196-202, 204–218, as being important for whole HK binding²⁷. To determine the location of the recombinant HKD5 and D5-1, D5-2 fragment binding sites we prepared four similar gC1qR variants removing negatively charged residues from the anionic loop regions; gC1qR-G2-5Ala (residues 146-148 and 156-157 mutated to Ala), gC1qRdelG3 (G3-loop residues 214-224 deleted), gC1qRdelG1 (G1-loop residues 196-200 deleted), and a G1-loop variant (residues 196-200) with five acidic residues substituted for

Ala termed gC1qR-G1-5Ala (Supplemental Figure 6). ITC experiments revealed only the gC1qRdelG3 variant had a significant effect in abrogating binding of HKD5 with other variants reproducing the multi-phase binding isotherms evident for *wt*-gC1qR (Figure 5a-c). We repeated the titration with the fragments D5-1 and D5-2 and observed no detectable binding to D5-1 and significant attenuation of binding to D5-2 (Figure 5b,c). This indicates that the central acidic G3-loop which defines an inner pocket (G3-pocket) plays a significant role in the interaction with HKD5, particularly for the binding of the N-terminal D5-1 region (Figure 5d, Video4). The placement of the G3-loop at the center of the gC1qR trimer is consistent with the allosteric nature of HKD5 and D5-1 binding as steric occlusion would reduce the ability of subsequent HKD5 ligands to co-bind (Figure 5e). Overall the anatomy of the gC1qR monomer is such that it resembles a hand with the FXII binding site formed between the index finger (G1-loop) and the thumb (α B) and the palm of the hand contains the Zn^{2+} binding site adjacent to which is the little finger (G3-loop), defining the principal HK binding site (Figure 5d, Video4).

Isolation of a gC1qR-HK-FXII ternary complex

As both HKD5 and the FXIIFnII domain exhibit asymmetric binding to the gC1qR trimer but by different mechanisms we next tested whether the FXIIFnII and HKD5 could bind simultaneously to gC1qR. If an excess of HKD5 is present then FXIIFnII cannot compete for binding, and this is consistent with multiple interaction sites for HKD5 identified by ITC. However, lower stoichiometric ratios of HKD5 reveal both HKD5 and FXIIFnII co-eluting in fractions from the gC1qR complex peak shown in Figure 6a. We next extended these studies to a series of gel filtration experiments using the full-length plasma purified FXII and HK in isolation and in combination with gC1qR. The molecular weights of FXII, HK and gC1qR estimated by reducing SDS-PAGE migration are 80kDa, 110kDa and 33kDa respectively and equivalent gel filtration estimates are 80kDa (FXII monomer), 200kDa (HK dimer³⁹) and 90kDa (gC1qR trimer). A mixture of full-length FXII, HK and gC1qR in the presence of Zn^{2+} resulted in co-migration of all three proteins in a single peak corresponding to a ~500kDa complex (Figure 6b). The stoichiometry of the species in this peak is equivalent to a 1:2:6 ratio of FXII-HK-gC1qR shown schematically in Figure 6c. The concept of a ternary complex formed

by FXII-HK-gC1qR is consistent with previous *in vitro* experiments by Joseph *et al.* showing that efficient gC1qR stimulation of PKa enzymatic activity requires the presence of PK, FXII, co-factor HK and Zn²⁺ ions⁴⁰.

gC1qR effects on plasma coagulation

We next tested the effects of gC1qR on plasma coagulation in the absence of additional stimuli and observed a dose-dependent shortening of clotting time with PNP in the presence of Zn²⁺ (Figure 7a). Thrombin generation experiments revealed a significant shortening in the lag time on addition of gC1qR and Zn²⁺ to PNP which influenced several additional parameters, including peak thrombin, endogenous thrombin potential and velocity of thrombin generation (Figure 7b-f). The lagtime of thrombin generation in the presence of gC1qR and Zn²⁺ was delayed by a factor of 2.8 in FXII-deficient plasma and absent in FXI-deficient plasma indicating a dependence on the intrinsic pathway (Figure 7c). Peerschke *et al.*, also showed that gC1qR did stimulate plasma coagulation but not in a FXII dependent manner⁴¹ and the reason for this discrepancy may relate to the addition of Zn²⁺. Analysis of two gC1qR variants revealed that the gC1qRdelG3 variant (but not gC1qRdelG1) was unable to stimulate thrombin generation to the same degree as *wt*-gC1qR implicating the central G3 loop as being functionally important for stimulation of coagulation. It is unknown whether the concentration of endothelial cell bound gC1qR is high enough to support thrombin generation on the vessel wall.

Discussion

How the contact factors assemble on the cell surface and become activated remains one of the fundamental and unanswered questions underpinning several pathways driving inflammation and thrombosis. The FXIIFnII-gC1qR-Zn²⁺ complex provides the first structural insight into a gC1qR ligand interaction and shows a stoichiometry of one FXIIFnII bound to the gC1qR trimer. The asymmetry of FXII binding to gC1qR involves two negatively charged surface pockets whereas for HKD5 this is driven by the central location of a critical negatively charged loop and steric occlusion. Overall the gC1qR ligand binding mode we observe for FXII and HK is consistent with the molecular

mechanism observed for the chaperone heat shock protein 90 (HSP90) whereby multiple client proteins can be co-localized by asymmetric binding onto the HSP90 dimer⁴². The parallel with HSP90 is pertinent as extracellular HSP90 has been described as a chaperokine⁴³ involved in inflammatory processes and was shown to initiate PK-HK activation⁴⁴. gC1qR has a requirement for FXII, PK and HK whereas HSP90 does not require FXII but only PK and HK⁴⁴.

FXII and HK binding to gC1qR is Zn^{2+} dependent and our data show Zn^{2+} is bound to gC1qR residues Asp185 and His187 in between the FXII and HK binding pockets (Video4). These observations build on data from Kumar *et al.* that describes a Zn^{2+} dependent conformational change in gC1qR²⁸ and thus provides an allosteric mechanism for modulation of the interaction with FXII. The biological context of Zn^{2+} modulation of the FXII-gC1qR interaction is proposed to originate from activated endothelial cells or secreted platelet granules^{45,46}. How gC1qR is anchored to the cell membrane has been reported to occur via interaction with other cell receptors¹ or cytokeratin-1⁴. uPAR has also been shown to act as a receptor for FXII and this interaction has been studied for endothelial⁴⁶, neutrophil⁴⁷ and dendritic cell⁴⁸ function. It is unknown whether gC1qR, uPAR and cytokeratin mediated binding of contact factors is functionally aligned.

Gel filtration using the full-length proteins identified a FXII-HK-gC1qR complex with an overall molecular weight in the 500kDa range which may represent FXII bound to two gC1qR trimers and a HK dimer (Figure 6c). The ability of gC1qR to cluster FXII and HK into a planar ternary complex is conceptually familiar to the way Vitamin K-dependent hemostatic proteases from the extrinsic pathway have their protease domains aligned with the substrate activation loop by a Ca^{2+} -dependent process on a planar phospholipid surface⁴⁹. Targeting a chaperone to disable the function of client proteins involved in a pathogenic mechanism is established for chaperones protein disulphide isomerase⁵⁰ and HSP90⁴² and our data provides a scaffold for a similar approach to target gC1qR¹⁴.

Acknowledgements

This work was funded through British Heart Foundation grant RG/12/9/29775 awarded to JE. Part of this work was funded by the Centre for membrane proteins (COMPARE) grant to JE and an EPSRC

studentship to AS. We acknowledge the Diamond Light Source for provision of synchrotron radiation in using the beamline I03.

Authorship contributions

BGK performed the experiments with FXIIFnII and gC1qR. AS performed the experiments with HKD5 and gC1qR. BGK, AS, ID, KRM designed experiments, analyzed the data, and critically reviewed the manuscript. SU, NJM performed plasma based assays. MS, JE contributed to the design of experiments, analysis of the data, preparation of the figures and to the writing of the manuscript.

Conflict of interest Disclosure.

J. Emsley receives consultant's fees from several pharmaceutical companies.

References.

1. Pathak M, Kaira BG, Slater A, Emsley J. Cell Receptor and Cofactor Interactions of the Contact Activation System and Factor XI. *Front Med (Lausanne)*. 2018;5:66.
2. Stavrou E, Schmaier AH. Factor XII: what does it contribute to our understanding of the physiology and pathophysiology of hemostasis & thrombosis. *Thromb Res*. 2010;125(3):210-215.
3. Long AT, Kenne E, Jung R, Fuchs TA, Renne T. Contact system revisited: an interface between inflammation, coagulation, and innate immunity. *J Thromb Haemost*. 2016;14(3):427-437.
4. Joseph K, Tholanikunnel BG, Ghebrehiwet B, Kaplan AP. Interaction of high molecular weight kininogen binding proteins on endothelial cells. *Thromb Haemost*. 2004;91(1):61-70.
5. Colman RW, Pixley RA, Najamunnisa S, et al. Binding of high molecular weight kininogen to human endothelial cells is mediated via a site within domains 2 and 3 of the urokinase receptor. *J Clin Invest*. 1997;100(6):1481-1487.
6. Herwald H, Dedio J, Kellner R, Loos M, Muller-Esterl W. Isolation and characterization of the kininogen-binding protein p33 from endothelial cells. Identity with the gC1q receptor. *J Biol Chem*. 1996;271(22):13040-13047.
7. Joseph K, Ghebrehiwet B, Peerschke EI, Reid KB, Kaplan AP. Identification of the zinc-dependent endothelial cell binding protein for high molecular weight kininogen and factor XII: identity with the receptor that binds to the globular "heads" of C1q (gC1q-R). *Proc Natl Acad Sci U S A*. 1996;93(16):8552-8557.
8. Yagi M, Uchiumi T, Takazaki S, et al. p32/gC1qR is indispensable for fetal development and mitochondrial translation: importance of its RNA-binding ability. *Nucleic Acids Res*. 2012;40(19):9717-9737.
9. Ghebrehiwet B, Lim BL, Peerschke EI, Willis AC, Reid KB. Isolation, cDNA cloning, and overexpression of a 33-kD cell surface glycoprotein that binds to the globular "heads" of C1q. *J Exp Med*. 1994;179(6):1809-1821.

10. Soltys BJ, Kang D, Gupta RS. Localization of P32 protein (gC1q-R) in mitochondria and at specific extramitochondrial locations in normal tissues. *Histochem Cell Biol.* 2000;114(3):245-255.
11. van Leeuwen HC, O'Hare P. Retargeting of the mitochondrial protein p32/gC1qR to a cytoplasmic compartment and the cell surface. *J Cell Sci.* 2001;114(Pt 11):2115-2123.
12. Feng X, Tonnesen MG, Peerschke EI, Ghebrehiwet B. Cooperation of C1q receptors and integrins in C1q-mediated endothelial cell adhesion and spreading. *J Immunol.* 2002;168(5):2441-2448.
13. Hosszu KK, Valentino A, Vinayagasundaram U, et al. DC-SIGN, C1q, and gC1qR form a trimolecular receptor complex on the surface of monocyte-derived immature dendritic cells. *Blood.* 2012;120(6):1228-1236.
14. Ghebrehiwet B, Jesty J, Vinayagasundaram R, et al. Targeting gC1qR domains for therapy against infection and inflammation. *Adv Exp Med Biol.* 2013;735:97-110.
15. Lu PD, Galanakis DK, Ghebrehiwet B, Peerschke EI. The receptor for the globular "heads" of C1q, gC1q-R, binds to fibrinogen/fibrin and impairs its polymerization. *Clin Immunol.* 1999;90(3):360-367.
16. Jiang J, Zhang Y, Krainer AR, Xu RM. Crystal structure of human p32, a doughnut-shaped acidic mitochondrial matrix protein. *Proc Natl Acad Sci U S A.* 1999;96(7):3572-3577.
17. Peerschke EI, Ghebrehiwet B. The contribution of gC1qR/p33 in infection and inflammation. *Immunobiology.* 2007;212(4-5):333-342.
18. Lim BL, Reid KB, Ghebrehiwet B, Peerschke EI, Leigh LA, Preissner KT. The binding protein for globular heads of complement C1q, gC1qR. Functional expression and characterization as a novel vitronectin binding factor. *J Biol Chem.* 1996;271(43):26739-26744.
19. Storz P, Hausser A, Link G, et al. Protein kinase C [micro] is regulated by the multifunctional chaperon protein p32. *J Biol Chem.* 2000;275(32):24601-24607.
20. Pathak M, Manna R, Li C, et al. Crystal structures of the recombinant beta-factor XIIa protease with bound Thr-Arg and Pro-Arg substrate mimetics. *Acta Crystallogr D Struct Biol.* 2019;75(Pt 6):578-591.
21. Dementiev A, Silva A, Yee C, et al. Structures of human plasma β -factor XIIa cocrystallized with potent inhibitors. *Blood Adv.* 2018;2(5):549-558.
22. Pathak M, Wilmann P, Awford J, et al. Coagulation factor XII protease domain crystal structure. *J Thromb Haemost.* 2015;13(4):580-591.
23. Beringer DX, Kroon-Batenburg LM. The structure of the F_NI-EGF-like tandem domain of coagulation factor XII solved using SIRAS. *Acta Crystallogr Sect F Struct Biol Cryst Commun.* 2013;69(Pt 2):94-102.
24. Clark CC, Hofman ZLM, Sanrattana W, den Braven L, de Maat S, Maas C. The Fibronectin Type II Domain of Factor XII Ensures Zymogen Quiescence. *Thromb Haemost.* 2020;120(3):400-411.
25. McCoy AJ, Grosse-Kunstleve RW, Adams PD, Winn MD, Storoni LC, Read RJ. Phaser crystallographic software. *J Appl Crystallogr.* 2007;40(Pt 4):658-674.
26. Murshudov GN, Skubák P, Lebedev AA, et al. REFMAC5 for the refinement of macromolecular crystal structures. *Acta Crystallogr D Biol Crystallogr.* 2011;67(Pt 4):355-367.
27. Ghebrehiwet B, Jesty J, Xu S, et al. Structure-function studies using deletion mutants identify domains of gC1qR/p33 as potential therapeutic targets for vascular permeability and inflammation. *Front Immunol.* 2011;2.

45. Fernando LP, Natesan S, Joseph K, Kaplan AP. High molecular weight kininogen and factor XII binding to endothelial cells and astrocytes. *Thromb Haemost.* 2003;90(5):787-795.
46. Mahdi F, Madar ZS, Figueroa CD, Schmaier AH. Factor XII interacts with the multiprotein assembly of urokinase plasminogen activator receptor, gC1qR, and cytokeratin 1 on endothelial cell membranes. *Blood.* 2002;99(10):3585-3596.
47. Stavrou EX, Fang C, Bane KL, et al. Factor XII and uPAR upregulate neutrophil functions to influence wound healing. *J Clin Invest.* 2018;128(3):944-959.
48. Göbel K, Pankratz S, Asaridou CM, et al. Blood coagulation factor XII drives adaptive immunity during neuroinflammation via CD87-mediated modulation of dendritic cells. *Nat Commun.* 2016;7:11626.
49. Pomowski A, Ustok FI, Huntington JA. Homology model of human prothrombinase based on the crystal structure of Pseutarin C. *Biol Chem.* 2014;395(10):1233-1241.
50. Cho J, Furie BC, Coughlin SR, Furie B. A critical role for extracellular protein disulfide isomerase during thrombus formation in mice. *J Clin Invest.* 2008;118(3):1123-1131.

FXIIFnII-gC1qR	
Data collection	
Space group	I121
Cell dimensions	
a, b, c (Å)	106.3, 71.6, 115.9
α , β , γ (°)	90, 110.6, 90
Resolution (Å)	91.0-3.1
R_{merge} (%) ^a	10.9 (45.5)*
$I / \sigma I$	7.1 (4.2)*
Completeness (%)	99.9 (100.0)*
Redundancy	3.1 (3.1)*
Wavelength	0.97949 Å
Refinement	
No. Reflections	14378
$R_{\text{work}}^b / R_{\text{free}}$ (%)	0.192/0.250
No. atoms	
Protein	4752
Zn ²⁺	3
Water	10
B -factors (Å ²)	
Protein	76.8
Metal	72.1
Water	46.7
R.m.s. deviations	
Bond lengths (Å)	0.012
Bond angles (°)	1.57

Table 1: Crystallographic data collection and refinement statistics.

*Values in parentheses are for highest-resolution shell.

^a $R_{\text{merge}} = \text{Sum}(h) [\text{Sum}(j) [I(hj) - \langle Ih \rangle] / \text{Sum}(hj) \langle Ih \rangle$ where I is the observed intensity and $\langle Ih \rangle$ is the average intensity of multiple observations from symmetry-related reflections calculated.

^b $R_{\text{work}} = \text{Sum}(h) ||F_o|_h - |F_c|_h| / \text{Sum}(h)|F_o|_h$, where F_o and F_c are the observed and calculated structure factors, respectively. R_{free} computed as in R_{work} , but only for (5%) randomly selected reflections, which were omitted in refinement, calculated using REFMAC.

	Binding model	N value	K_D (nM)	ΔH (kJ mol ⁻¹)	ΔS (J K ⁻¹ M ⁻¹)	ΔG (kJ mol ⁻¹)
D5	3 Site sequential binding	-	1) 1.9 (\pm 0.1)	1) -268.8 (\pm 1.1)	1) -732.7	1) -50.5
2) 64.9 (\pm 1.9)			2) -105.2 (\pm 1.3)	2) -214.8	2) -41.2	
3) 1011.1 (\pm 75.8)			3) -23.5 (\pm 1.4)	3) 36.0	3) -34.3	
D5-1	3 Site sequential binding	-	1) 73.0 (\pm 4.0)	1) -200.9 (\pm 1.4)	1) -535.9	1) -41.2
2) 1579.8 (\pm 145.3)			2) -92.2 (\pm 4.9)	2) -198.5	2) -33.0	
3) 2673.8 (\pm 257.7)			3) -62.2 (\pm 5.9)	3) -101.7	3) -31.9	
D5-2	Single site	2.30 (\pm 0.01)	763.4 (\pm 27.5)	-1459.1 (\pm 1.1)	-382.7	-35.1
HK 496-516	Single site	2.56 (\pm 0.02)	1612.9 (\pm 90.3)	-164.0 (\pm 1.8)	-439.6	-33.2

gC1qR construct	D5 construct	N value	K_{D1} (nM)	K_{D2} (nM)	K_{D3} (nM)
<i>wt</i>	D5	-	1.9 (\pm 0.1)	64.9 (\pm 1.9)	1011.1 (\pm 75.8)
G2-5Ala	D5	-	1.2 (\pm 0.1)	33.4 (\pm 5.7)	724.6 (\pm 178.3)
DelG1	D5	-	1.5 (\pm 0.2)	44.8 (\pm 6.0)	1283.7 (\pm 238.8)
G1-5Ala	D5	-	3.4 (\pm 0.4)	120.3 (\pm 11.5)	1083.4 (\pm 176.6)
DelG3	D5	-		No fit	
<i>wt</i>	D5-1	-	73.0 (\pm 4.0)	1579.8 (\pm 145.3)	2673.8 (\pm 257.7)
G2-5Ala	D5-1	-	131.1 (\pm 43.0)	1084.6 (\pm 517.4)	3663.0 (\pm 369.1)
DelG1	D5-1	-	135.8 (\pm 37.3)	1228.5 (\pm 407.9)	3690.0 (\pm 638.4)
G1-5Ala	D5-1	-	120.8 (\pm 55.4)	680.3 (\pm 420.0)	1557.3 (\pm 369.1)
DelG3	D5-1	-		No fit	
<i>wt</i>	D5-2	2.3 (\pm 0.01)	763.4 (\pm 27.5)		
G2-5Ala	D5-2	2.1 (\pm 0.02)	885.0 (\pm 31.9)		
DelG1	D5-2	2.3 (\pm 0.03)	724.6 (\pm 50.0)		
G1-5Ala	D5-2	2.3 (\pm 0.02)	800.0 (\pm 45.6)		
DelG3	D5-2	0.5 (\pm 0.02)	2032.5 (\pm 233.7)		

Table 2: ITC binding measurements of the HKD5 interaction with gC1qR. ITC-derived thermodynamic properties for the binding of HKD5, D5-1 and D5-2 with gC1qR, and individual K_D values for the binding of HKD5 to the *wt*-gC1qR and gC1qR variant proteins. N values are not provided for the three site sequential binding fits as the stoichiometry is fixed at three.

FIGURE LEGENDS

Figure 1. Structure of FXII, gC1qR and HK. (a) Domain organization of FXII, gC1qR and HK. The gC1qR anionic loops are red and residue numbers for domain boundaries are labeled. (b) Gel filtration elution profiles for FXIIFnII (blue) and gC1qR (black) in isolation and a gC1qR-FXIIFnII mixture (red). (c) Coomassie stained SDS-PAGE gel of the fractions collected from gel filtration of the FXIIFnII-gC1qR mixture. Lanes labelled 15-18 correspond to elution volumes 15-18ml from (b) showing both proteins co-eluting as a complex with excess FXIIFnII observed at 20ml. The first lane labelled M is the protein marker and the second lane is gC1qR in isolation. (d) Cartoon diagram of the FXIIFnII-gC1qR complex crystal structure showing the FXIIFnII domain (cyan) in complex with gC1qR (wheat, purple, green) with Zn^{2+} in blue and the anionic G1-loop in red and key interacting side chains as sticks. (e) Space filling representation of the gC1qR complex with the FXIIFnII domain as spheres (cyan) with residues Arg36 and Arg65 in orange.

Figure 2. Structure of the FXIIFnII domain gC1qR interface. (a) Cartoon diagram of the FXIIFnII-gC1qR complex colored as in Figure 1e. The gC1qR G1-loop, residues 196-204 (red) and pockets G1 and G2 are labelled interacting with FXII residues Arg36 and Arg65 (orange) shown as sticks. Electrostatic interactions are shown as purple dotted lines and the Zn^{2+} as a blue sphere. (b) Interactions of the gC1qR G1-loop with FXII are shown as two different views. (c) gC1qR G2-pocket is shown (purple) and key interacting FXII residues are shown as sticks and gC1qR residue Trp233 as sticks (wheat). (d) A charged surface representation of the gC1qR G1 and G2-pockets with FXIIFnII in cyan as a cartoon diagram with key interacting side chains as sticks.

Figure 3. Quantitation of gC1qR binding to FXII using SPR. Plots of SPR sensorgrams measured in response units (RU) on the y-axis are shown illustrating *wt*-gC1qR (a) and gC1qR variants (b-d) binding to immobilized full-length FXII at increasing concentrations indicated. (b) gC1qR variant with four Ala substitutions made in the region of the G1-pocket (T228A, D229A, W233A, Y236A). (c) gC1qR G2-pocket variant (S106A, D249A) and (d) gC1qR variant H187A (Zn^{2+} binding site

ablation). (e) Cartoon diagram showing a close up view of the gC1qR Zn^{2+} binding site with key residues shown as sticks and electrostatic interactions shown as dashed lines (purple). The Zn^{2+} (grey) and water molecules (red) are shown as solid spheres. (f) Superposition of the FXIIFnII bound gC1qR (colored wheat with the FXII side chain Arg36 in orange) with the unbound gC1qR structure (cyan) in the region of the G1-pocket illustrating conformational changes. The Arg207 side chain replaces the Zn^{2+} in coordinating the Asp185 side chain in the ligand free gC1qR structure. Black arrows indicate gC1qR side chain movements from ligand free to FXIIFnII bound. Electrostatic interactions are shown as purple dotted lines.

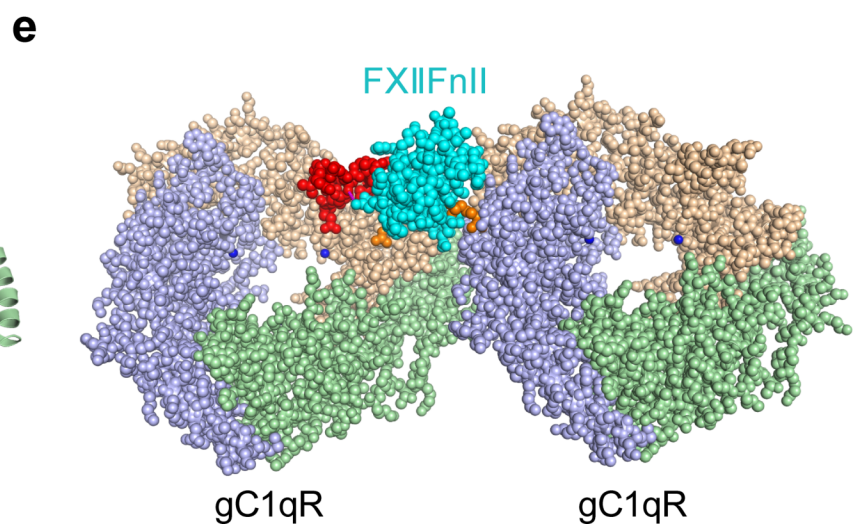
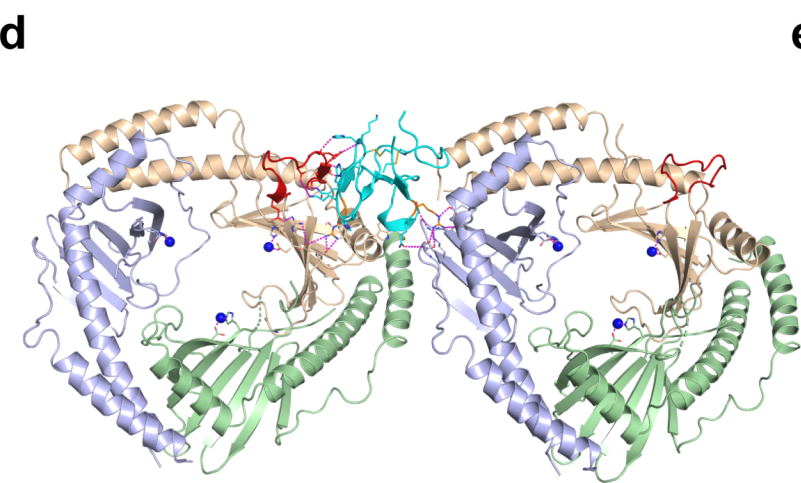
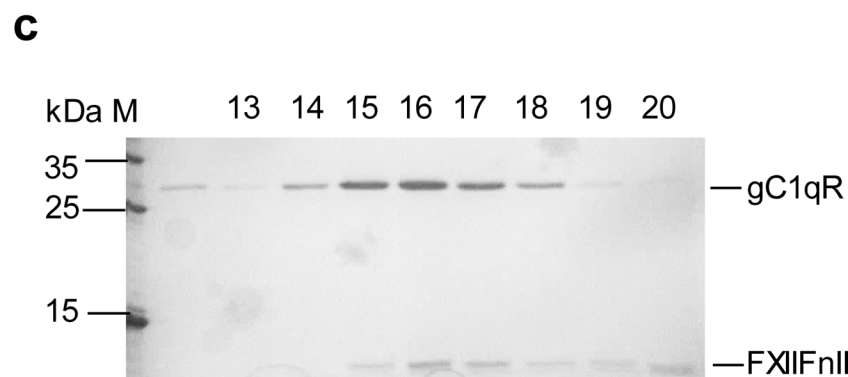
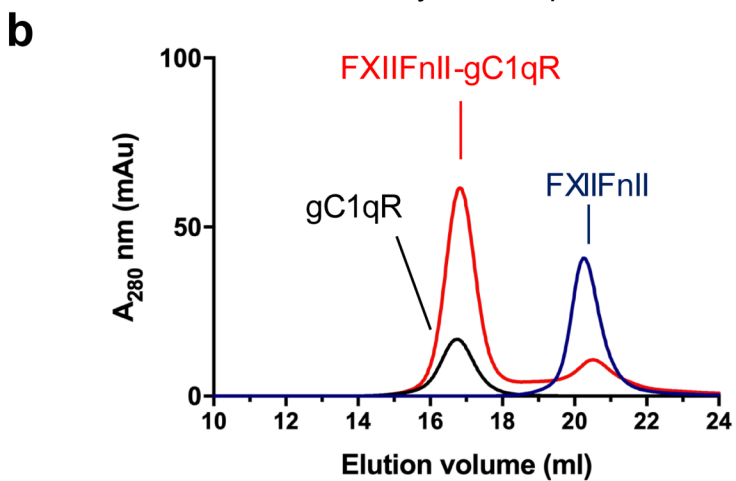
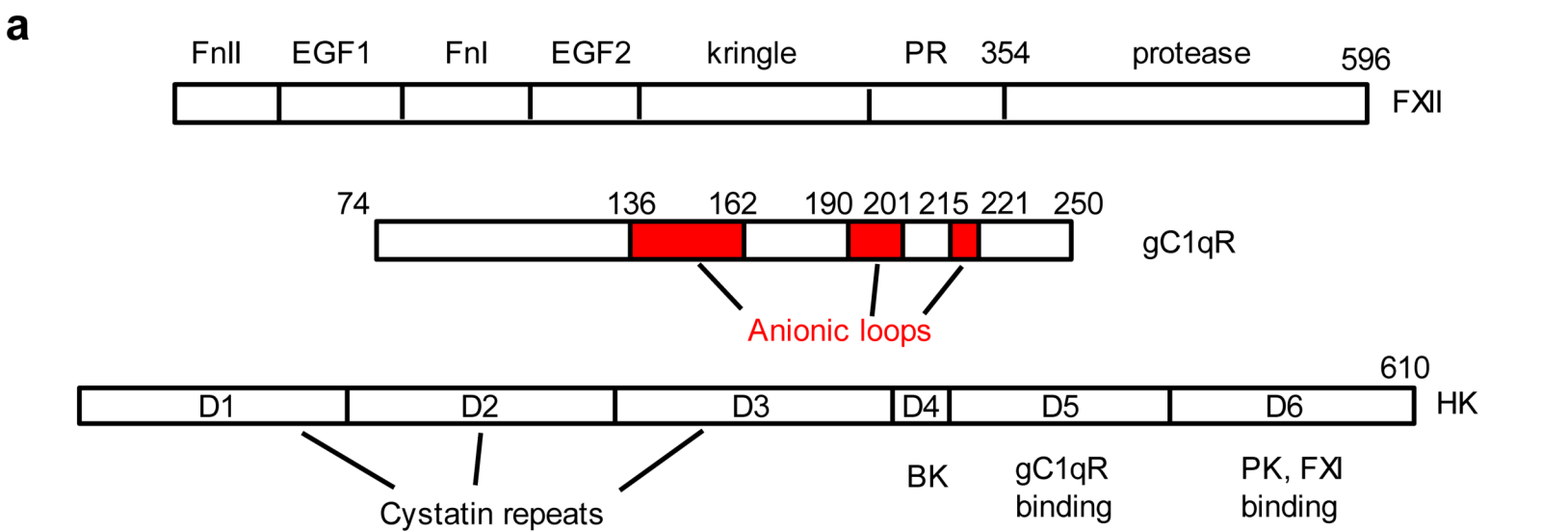
Figure 4. Analysis of gC1qR binding to HKD5. (a) The recombinant HKD5 construct boundaries are shown with residue numbers indicated for D5-1, D5-2 and shorter peptides used in the ITC and gel filtration experiments. (b) Gel filtration of HKD5 combined with gC1qR at different molar ratios. Elution profiles on the left, and coomassie stained SDS-PAGE gels of the fractions collected are shown on the right. The 3:1 ratio of HKD5 to gC1qR reveals excess HKD5 eluting separately suggesting the trimer only supports two HKD5 polypeptides. (c) ITC measurements of gC1qR binding to HKD5. D5 was titrated into gC1qR in the presence of Zn^{2+} or EDTA. This was fit to a three site-sequential binding model with no difference between curves produced in the presence or absence of Zn^{2+} . (d) Gel filtration of D5-1, D5-2 and gC1qR in the presence of 50 μ M $ZnCl_2$ (black) or 5 mM EDTA (red) revealing D5-1 has a Zn^{2+} dependence whereas HKD5-2 does not. (e) ITC experiments with D5-1 and D5-2 respectively titrated into gC1qR in the presence of Zn^{2+} . Similarly to full-length HKD5, D5-1 was fitted to a three site-sequential binding model and binding was Zn^{2+} -dependent. (f) The binding of D5-2 was Zn^{2+} -independent and was fit to a single site binding model with a calculated N value of 2. (g) HKD5 derived shorter peptides titrated into gC1qR. All titrations excluding HK 493-516 were performed in the presence of Zn^{2+} . HK 493-516 was the only peptide to show binding and the curve resulted in comparable binding affinities and N values to D5-2.

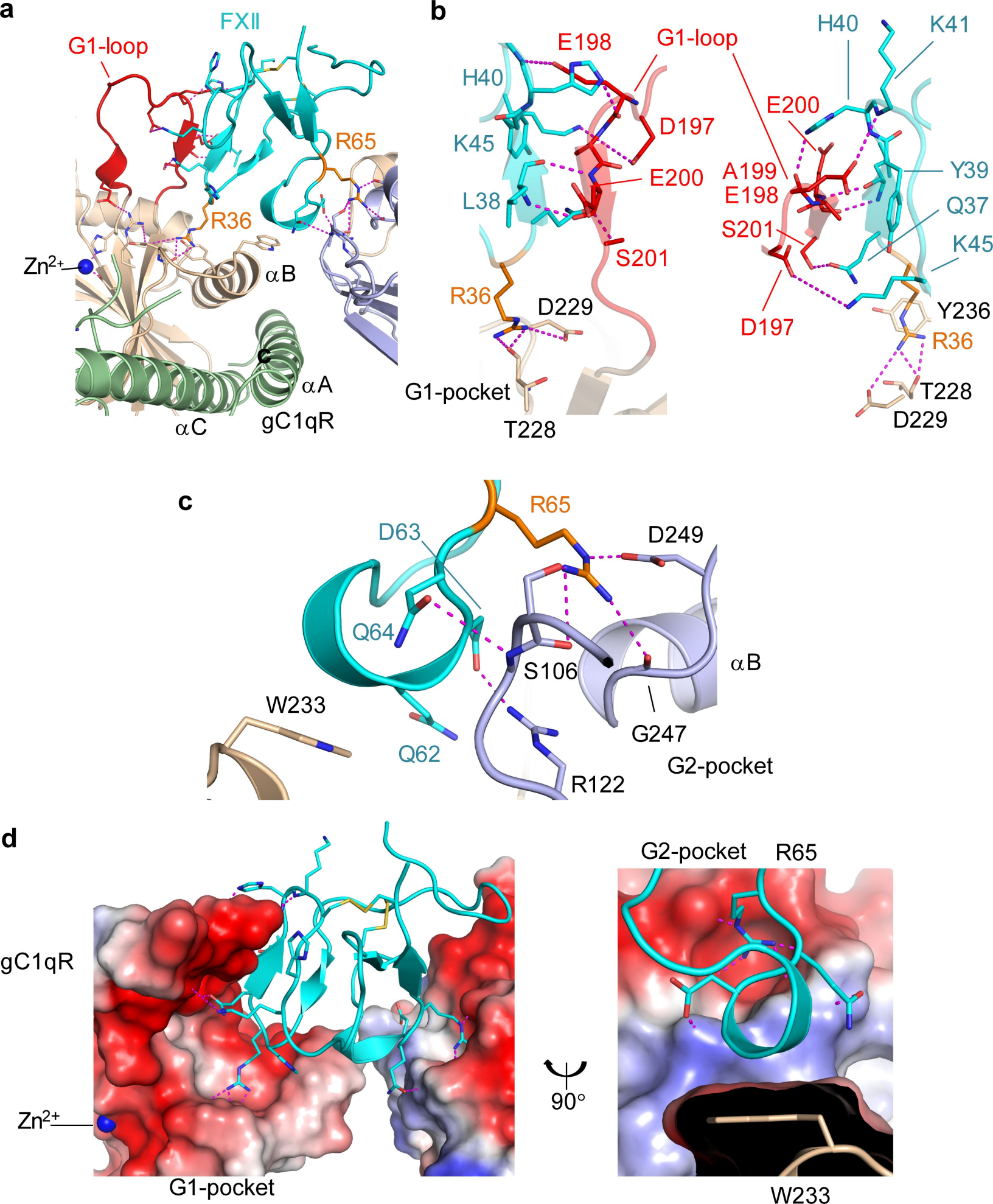
Figure 5. Mapping of the gC1qR binding site for HKD5. (a,b,c) ITC experiments with HKD5, D5-1 and D5-2, respectively titrated against the gC1qR variants compared with *wt*-gC1qR. Deletion of

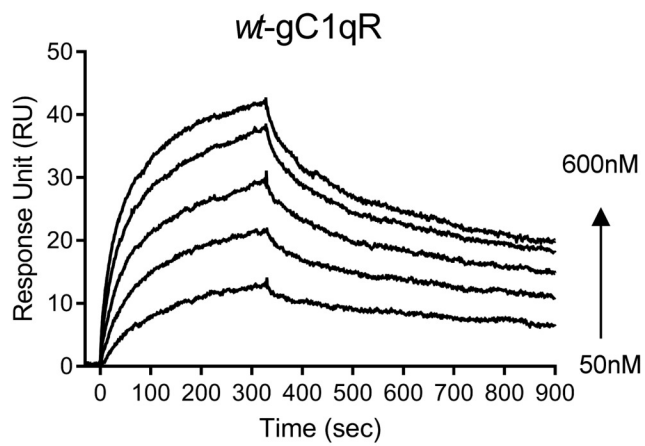
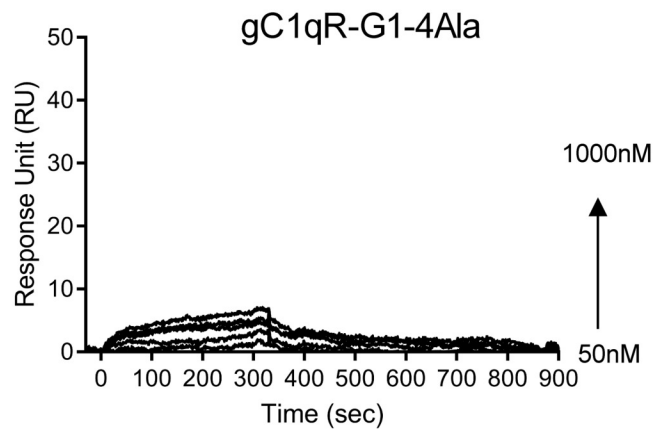
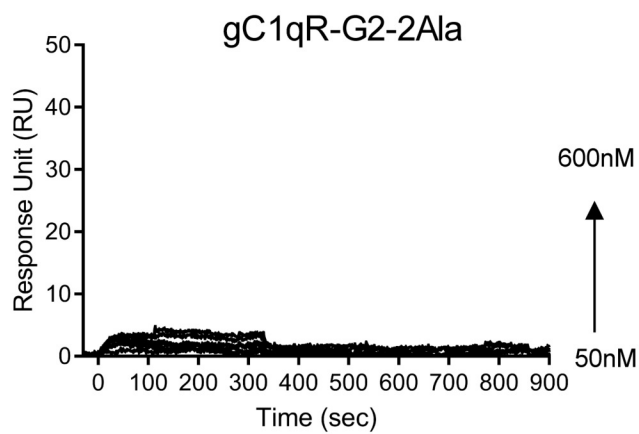
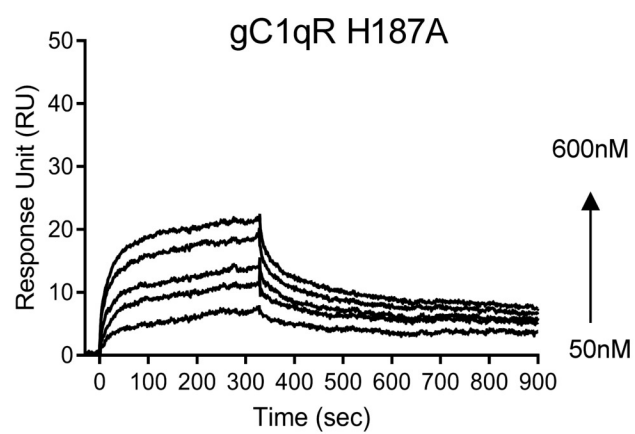
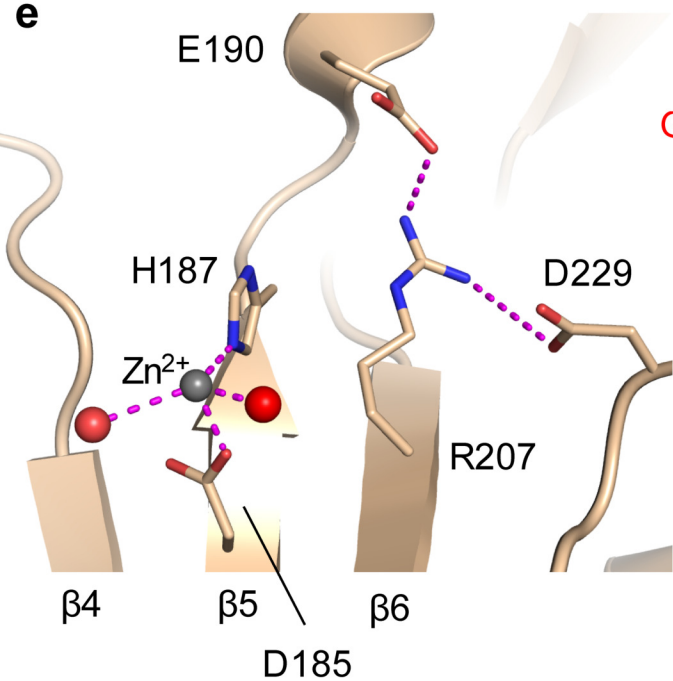
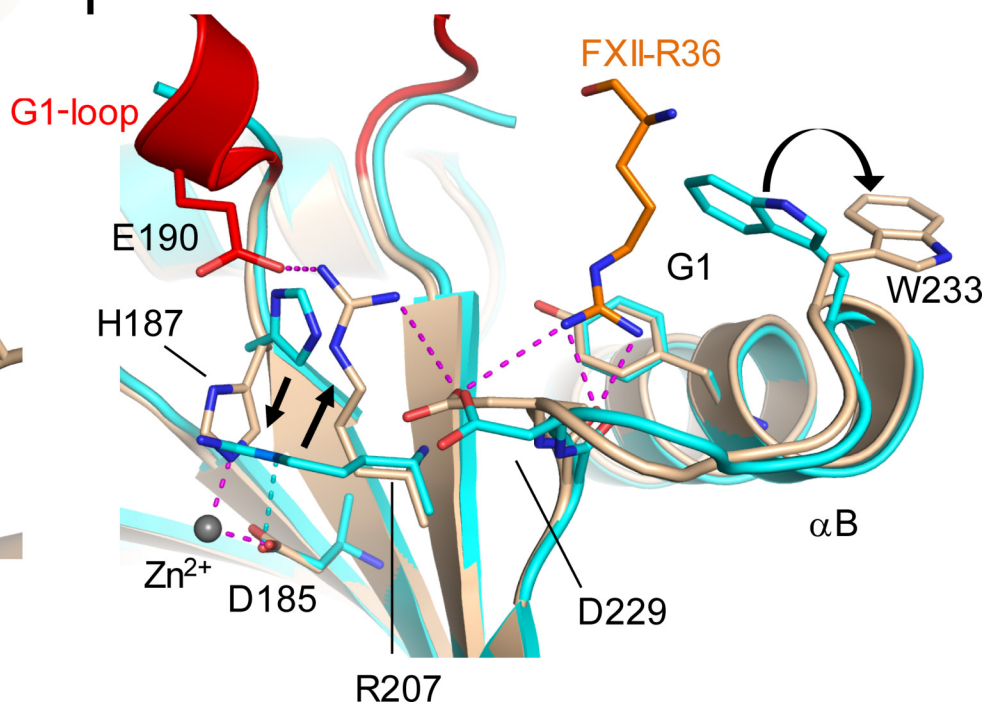
the gC1qR G3-loop (gC1qRdelG3) in blue showed no binding to D5-1 and reduced binding to both HKD5 and D5-2 whereas the other variants were comparable to *wt*-gC1qR. (d) The HKD5 binding site maps to the region of the G3-loop (blue) which forms the boundary of a pocket (G3, shown as blue dashed ellipse) which extends across the β -sheet to the Zn^{2+} site (grey sphere). The location of the G1-pocket is shown (purple dashed ellipse) and G2-loop (orange), G1-loop (red). (e) A schematic representation of the proposed D5 binding to gC1qR. The ligand free gC1qR and HKD5 are shown top left. D5-1 is represented as a larger circle (blue) connected to a smaller circle representing D5-2 (red). The larger size of the D5-1 circle is representative that this region binding to gC1qR cannot be emulated by short peptides. gC1qR is shown in grey to represent the Zn^{2+} free form and flexible anionic loops are shown colored as in (d) with the G1 and G2-loops radially located and the G3-loop in the centre. The binding of D5-1 is sequential whereby tight binding of the first D5-1 (K_{D1}) is followed by subsequently reduced affinity second and third binding events (K_{D2} , K_{D3}) suggesting a third HKD5 binding is sterically occluded (shown as transparent). The binding of D5-2 to gC1qR is not sequential and all binding events to gC1qR have equivalent affinity (K_{D1}).

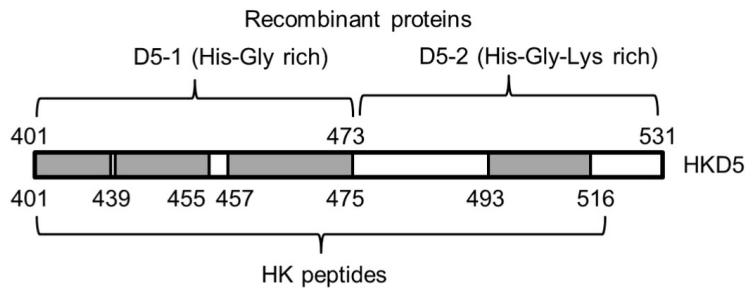
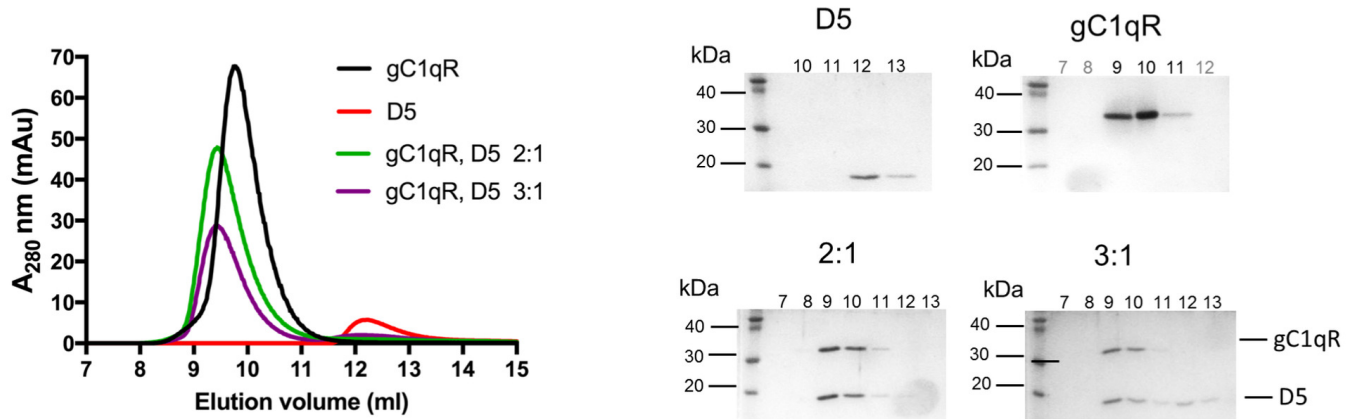
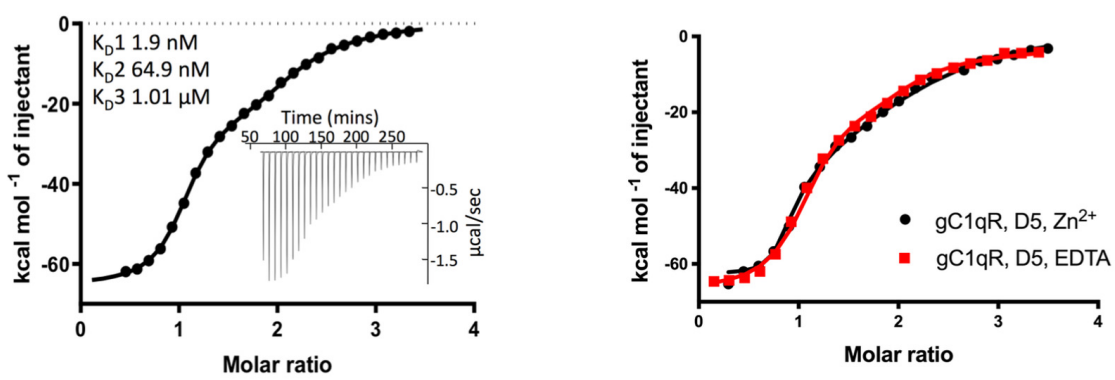
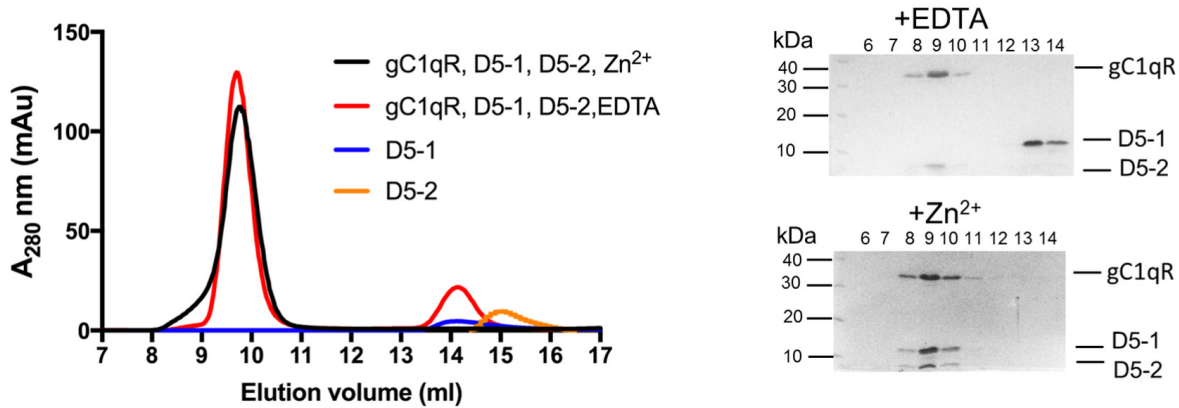
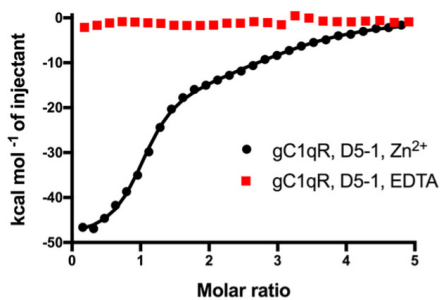
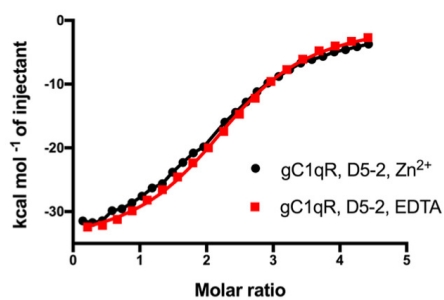
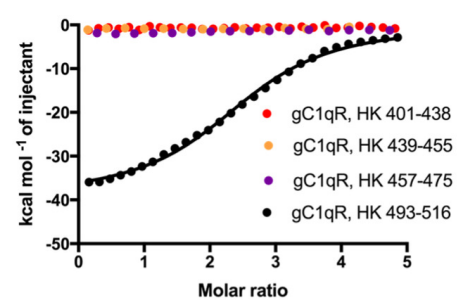
Figure 6. Ternary complexes of FXII, HK and gC1qR analysed by gel filtration. (a) Analytical gel filtration elution profiles showing FXIIFnII, D5 and gC1qR combined with increasing concentrations of HKD5 in the presence of Zn^{2+} . On the right coomassie stained SDS-PAGE gels showing gC1qR, HKD5 and FXIIFnII in the fractions collected. As the concentration of HKD5 is increased, FXIIFnII shifts from the high molecular weight peak to the low molecular weight peak suggesting D5 is outcompeting FXIIFnII for gC1qR binding. (b) Analytical gel filtration (Superose 6 10/300) of full-length proteins HK (green), FXII (blue), gC1qR (black), and the gC1qR-HK-FXII ternary complex (red). Coomassie stained SDS-PAGE gel showing the peak fraction of the gC1qR-HK-FXII ternary complex. (c) Schematic diagram of a hypothetical FXII-HK-gC1qR-PK complex with a 1:2:6:2 stoichiometry. In this model gC1qR is capable of stimulating reciprocal FXII-PK activation by aligning the activation loops and active sites of the FXII and PK proteases.

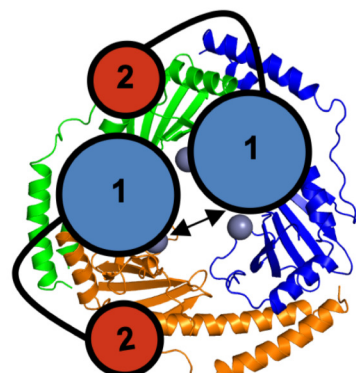
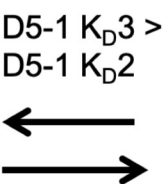
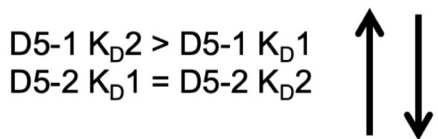
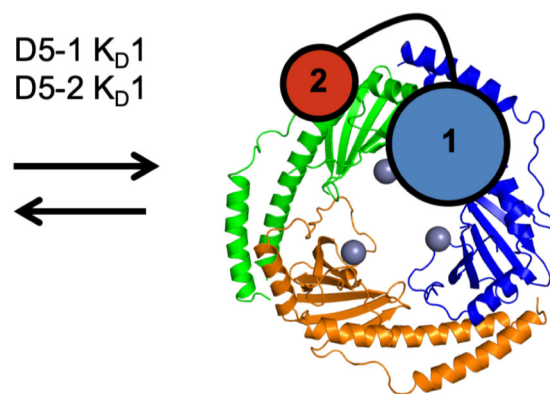
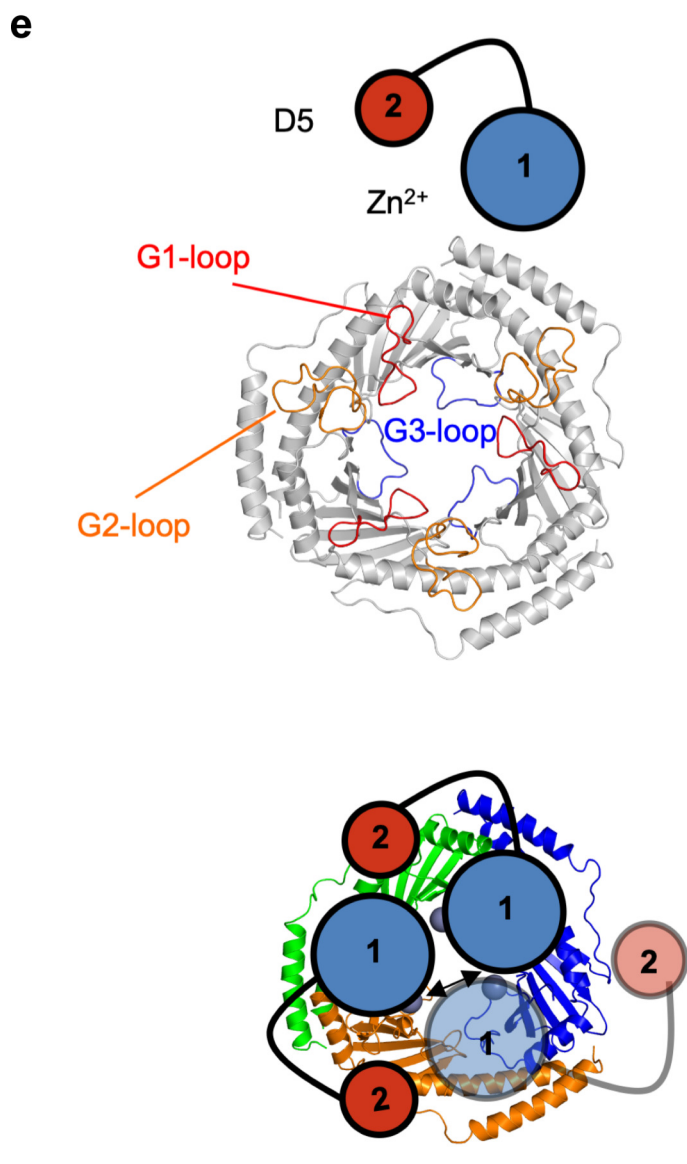
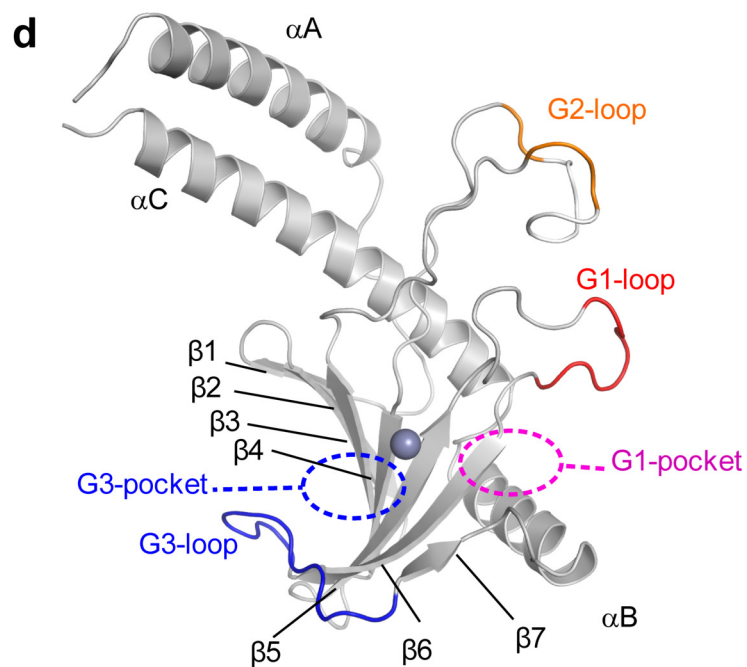
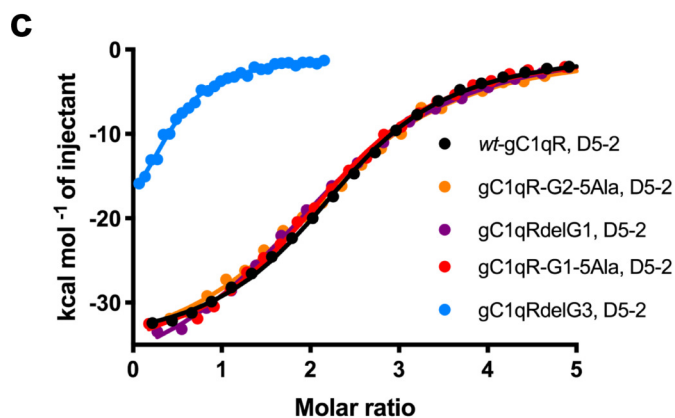
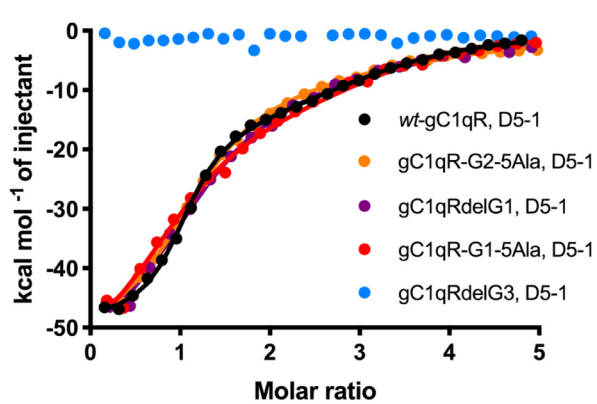
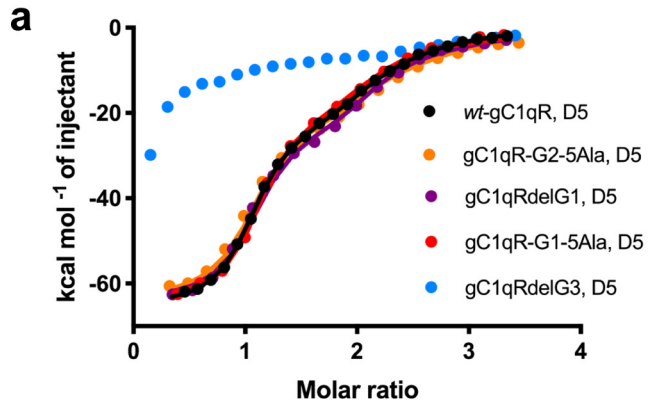
Figure 7. gC1qR stimulation of plasma coagulation in a FXII dependent manner. (a) PNP was incubated with MP reagent for 180 s and increasing concentrations of gC1qR (50-200 $\mu\text{g/ml}$) with Zn^{2+} (50 μM). Coagulation was initiated by addition of CaCl_2 (8.3 mM) and clotting time monitored. (b-f) Thrombin generation for PNP with gC1qR (50-200 $\mu\text{g/ml}$) and Zn^{2+} (50 μM); (b) raw data curves in the presence of gC1qR (orange) and without (grey) (c) lagtime (min), (d) endogenous thrombin potential (ETP; nM.min), (e) peak thrombin (nM), and (f) velocity index (nM/min) were derived. (g) Lagtime (min) is shown for thrombin generation of PNP, FXII or FXI deficient plasma incubated \pm gC1qR (100 $\mu\text{g/ml}$) and Zn^{2+} (50 μM). In the absence of gC1qR there was no thrombin generation evident in FXI or FXII deficient plasma. FXII-deficient plasma with gC1qR shows a significant delay in thrombin generation with a lag time of 25 ± 6.7 min versus 9 ± 0.7 min in PNP and no thrombin generation in FXI deficient plasma iwth gC1qR indicating a dependence on the intrinsic pathway. (h) Lagtime (min) is shown for thrombin generation of PNP, gC1qR (100 $\mu\text{g/ml}$) and gC1qR variants with G1 (cyan) and G3-loops (pink) deleted showing a dependency on the gC1qR G3-loop.

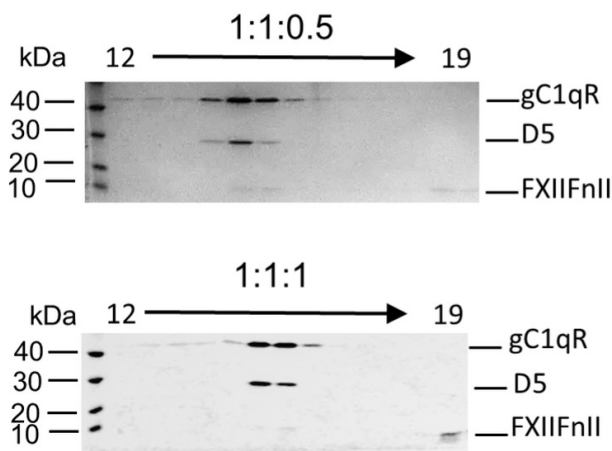
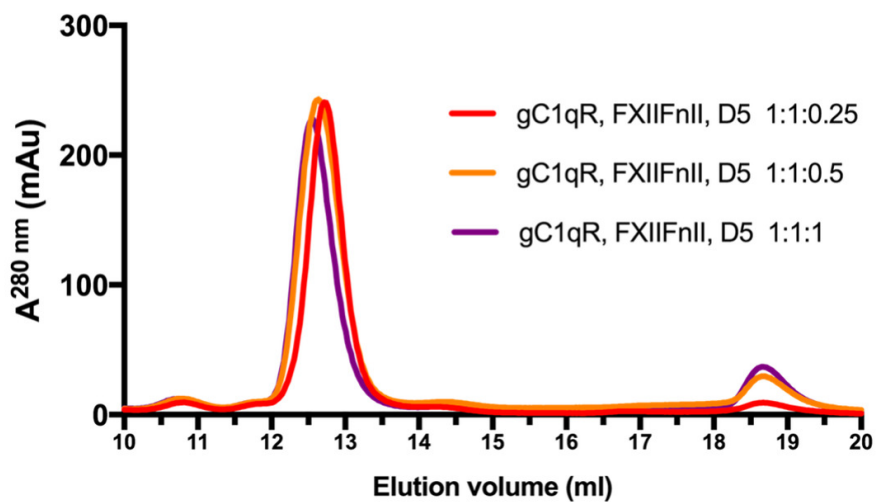
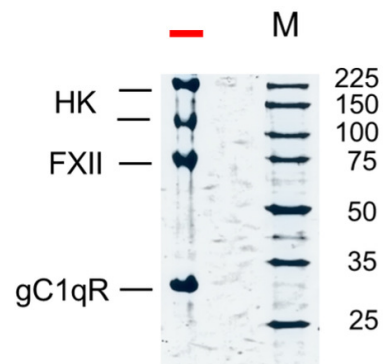
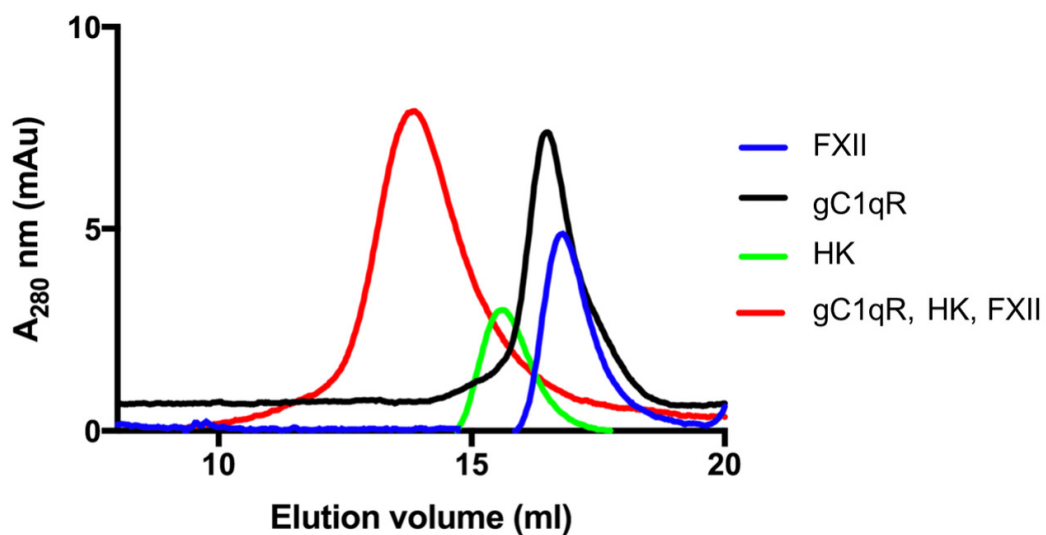




a**b****c****d****e****f**

a**b****c****d****e****f****g**



a**b****c**